MinE conformational dynamics regulate membrane binding, MinD interaction, and Min oscillation

Kyung-Tae Park[a], Maria T. Villar[b], Antonio Artigues[b], and Joe Lutkenhaus[a,1]

[a]Department of Microbiology, Molecular Genetics & Immunology, University of Kansas Medical Center, Kansas City, KS 66160; and [b]Department of Biochemistry and Molecular Biology, University of Kansas Medical Center, Kansas City, KS 66160

This contribution is part of the special series of Inaugural Articles by members of the National Academy of Sciences elected in 2014.

Contributed by Joe Lutkenhaus, June 6, 2017 (sent for review May 5, 2017; reviewed by Martin Loose and David S. Weiss)

In *Escherichia coli* MinE induces MinC/MinD to oscillate between the ends of the cell, contributing to the precise placement of the Z ring at midcell. To do this, MinE undergoes a remarkable conformational change from a latent 6β-stranded form that diffuses in the cytoplasm to an active 4β-stranded form bound to the membrane and MinD. How this conformational switch occurs is not known. Here, using hydrogen–deuterium exchange coupled to mass spectrometry (HDX-MS) we rule out a model in which the two forms are in rapid equilibrium. Furthermore, HDX-MS revealed that a MinE mutant (D45A/V49A), previously shown to produce an aberrant oscillation and unable to assemble a MinE ring, is more rigid than WT MinE. This mutant has a defect in interaction with MinD, suggesting it has difficulty in switching to the active form. Analysis of intragenic suppressors of this mutant suggests it has difficulty in releasing the N-terminal membrane targeting sequences (MTS). These results indicate that the dynamic association of the MTS with the β-sheet is fine-tuned to balance MinE's need to sense MinD on the membrane with its need to diffuse in the cytoplasm, both of which are necessary for the oscillation. The results lead to models for MinE activation and MinE ring formation.

Min oscillator | MinE | MinD | conformational dynamics | self-organization

In *Escherichia coli* the proteins that comprise the Min system (MinC, MinD, and and MinE) undergo a coupled oscillation that prevents Z ring assembly away from midcell (1). MinD is a peripheral membrane ATPase (2) that interacts with two partners, MinE and MinC (3–5). Interaction with MinE leads to the oscillation, whereas interaction with MinC, which is a passenger in the oscillation, leads to the formation of a potent antagonist of Z ring assembly (6). During the oscillation MinD and MinC form a polar zone on the membrane flanked by a MinE ring near midcell (7–9). As the MinE ring proceeds toward the occupied pole MinD and MinC are released and reassemble a new polar zone at the other pole that is again flanked by a MinE ring near midcell and the process repeats (10, 11). Key elements of the oscillation are the cooperative binding of MinD to the membrane, the recruitment of MinE, which displaces MinD, and the ability of MinE to processively remove MinD from the membrane (1, 12).

The oscillatory dynamics of the Min system are driven by the stimulation of MinD's ATPase by MinE (13). MinD dimerizes in the presence of ATP and binds to the membrane (4, 5, 14, 15). MinE, which is also a dimer, binds to MinD at the membrane, stimulating its ATPase and causing its release from the membrane (5, 15). Genetic and structural data revealed that MinE exists in two dramatically different conformations, designated the latent and active forms (16) (Fig. 1). The latent conformation is a 6β-stranded structure that diffuses in the cytoplasm because the segments of MinE that interact with MinD (β1 strand at the dimer interface) and the membrane (N-terminal amphipathic helices also called membrane targeting sequences, MTS) are masked. In contrast, the active conformation consists of a 4β-stranded structure with the MTS bound to the membrane and the released β1 strand and part of the loop region (residues 11–28) converted to an alpha helix bound to MinD (Fig. 1). How MinE is converted to the active form (i.e., the transition from the 6β- to the 4β-stranded form) is not clear, although it does not involve a monomer intermediate (17).

The latent form of MinE has a hydrophobic core with the six-stranded β-sheet sandwiched between the MTS on one face and two long antiparallel helices (αB) forming a coiled coil on the opposite face (18) (Fig. 1). The analysis of certain mutants has yielded information about MinE's conformational switch. The I25R mutation releases the MTS, causing constitutive membrane binding without disrupting the 6β-stranded structure, suggesting membrane binding is insufficient to flip the switch (16). Hydrophilic substitutions for residue I24 also cause constitutive membrane binding by forcing MinE into the 4β-stranded active form. By forcing MinE into the active form mutations like I24N suppress a subset of MinD mutants that are unresponsive to WT MinE (16). This led to a model in which MinE senses MinD, which promotes the 6β- to 4β-strand switch (i.e., MinE activation). This is in contrast to an equilibrium model in which the two forms of MinE interconvert spontaneously and the equilibrium is pulled toward the 4β form as a result of MinD binding.

Previously, a MinE mutant was described with two substitutions in exposed residues in the coiled coil (D45A and V49A) that was unable to restore a WT phenotype (19, 20) (Fig. 1). In addition, it produced a meandering and slow oscillation of MinD

Significance

The Min system is a well-studied biological oscillator that consists of MinC, MinD, and MinE. MinE assembles into a ring that drives a pole-to-pole oscillation of the FtsZ antagonist MinC/MinD to ensure positioning of the Z ring at midcell. To do this, MinE undergoes a remarkable conformational switch, but how it does this is not clear. Here, we use intragenic suppressors of a MinE mutant along with hydrogen–deuterium exchange to elicit the pathway for the conformational switch. The results lead to a multistep model that involves MinD and engenders an appreciation for how the MinE structure is fine-tuned to switch between a form that diffuses in the cytoplasm and a form that binds the membrane and, ultimately, MinD.

Author contributions: K.-T.P. and J.L. designed research; K.-T.P., M.T.V., and A.A. performed research; K.-T.P., M.T.V., A.A., and J.L. analyzed data; and K.-T.P. and J.L. wrote the paper.

Reviewers: M.L., Institute of Science and Technology Austria; and D.S.W., University of Iowa.

The authors declare no conflict of interest.

[1]To whom correspondence should be addressed. Email: jlutkenh@kumc.edu.

This article contains supporting information online at www.pnas.org/lookup/suppl/doi:10.1073/pnas.1707385114/-/DCSupplemental.

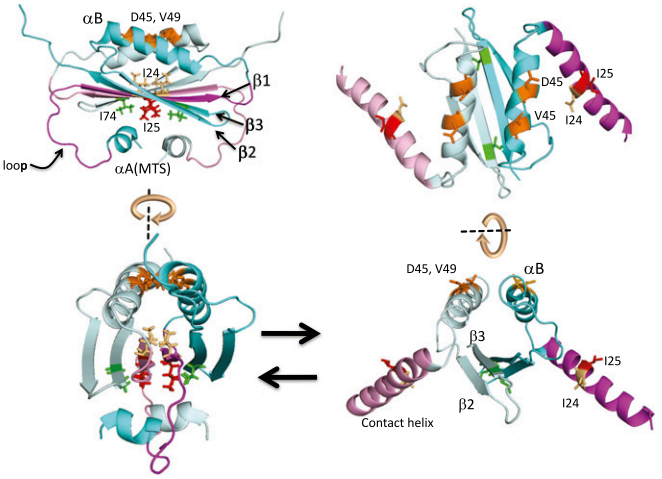

Fig. 1. Conformational changes associated with activation of MinE. The MinE dimer undergoes a dramatic conformational change from a latent 6β-stranded form [Protein Data Bank (PDB) ID code 2KXO] to an active 4β-stranded form (only MinE from the MinE-MinD complex is depicted, PDB ID code 3R9J). MinE is a dimer and the two subunits are indicated by darker and lighter shades of magenta and cyan. The region in magenta in the 6β-stranded form is converted to an α helix (contact helix) in the 4β-stranded form, which is stabilized by binding to MinD (not depicted). The 6β-stranded form has a hydrophobic core with a coiled coil (αB) on one side of the β-sheet and a MTS (αA) on the other. The MTS is tethered to the β-sheet by interaction with I25 and I74. Note that the MTS is not present in the 4β-stranded form, which starts at residue 12. The I24 residue is colored light orange, I25 is red, I74 is green, and D45 and V49 are dark orange.

and did not form a MinE ring. The basis for this behavior was unclear; however, we suspected that this MinE mutant was defective in conversion to the active form. Here we used hydrogen–deuterium exchange coupled to mass spectrometry (HDX-MS) to examine the conformational dynamics of MinE and this mutant to gain insight into the mechanism of MinE activation and the mutant defect. Our results support the previous model (16) and indicate that the first step is the release of the MTS. We propose that release of the MTS frees the loop region to interact with MinD, inducing it to form an alpha helix (the contact helix, Fig. 1) that propagates into the β1 strand and flips the switch. Our results suggest that dynamic tethering of the MTS to the β-sheet is fine-tuned and has a role in MinE ring formation.

Results

The MinE$^{D45A/V49A}$ and MinE^{D45A} Mutations Impair MinE Activity. Previous work found that a plasmid encoding *minC*, *minD*, and *minE$^{D45A/V49}$* could not restore a WT phenotype when introduced into a Δ*min* strain even though the mutant MinE was stable (19, 20). To further explore the effects of these mutations we transformed JS964 (Δ*min*) with pSEB104CD (P$_{BAD}$::*minC minD*) and pJB216E (P$_{lac}$::*minE*) or variants encoding either *minE^{D45A}* or *minE$^{D45A/V49A}$* and examined growth and cell morphology in the presence of 0.2% arabinose with or without isopropyl β-D-1-thiogalactopyranoside (IPTG). The basal level of MinE (no IPTG) partially suppressed the inhibitory activity of MinC/MinD, whereas the level induced by 10 μM IPTG completely suppressed and allowed colony formation (Fig. 2*A*). In contrast, JS964/pSEB104CD containing pJB216E-D45A/V49A (P$_{lac}$::*minE$^{D45A/V49A}$*) did not grow with 10 μM IPTG and grew poorly at 25 μM ITPG and cells were extremely filamentous. JS964/pSEB104CD containing pJB216E-D45A (P$_{lac}$::*minE^{D45A}*) did not grow at 10 μM IPTG but was able to form colonies at 25 μM IPTG. These results indicate that the D45A substitution reduces MinE activity, which is further reduced by the addition of the V49A mutation, in agreement with the previous report (19).

In the above test MinE was expressed in *trans*. A more physiological assessment of the effect of the mutations is to express them in *cis* in the context of the operon and at the physiological level. Therefore, pSEB104CDE (P$_{BAD}$::*minC minD minE*) and variants containing *minE$^{D45A/V49A}$* or *minE^{D45A}* were introduced into JS964 (Δ*min*). In the presence of 0.2% arabinose JS964/pSEB104CDE grew well and exhibited a WT morphology. Under these conditions the Min proteins are expressed near the physiological level (21). In contrast, JS964 containing pSEB104CDE-D45A/V49A or pSEB104CDE-D45A displayed poor colony formation in the presence of arabinose (Fig. 2*B*). Examination of a culture grown in LB medium for several hours after the addition of arabinose revealed highly filamentous cells, indicating that the two MinE mutants failed to overcome the inhibitory activity of MinC/MinD (Fig. 2*B*).

MinE$^{D45A/V49A}$ Is Defective in MinD Interaction. The above results clearly indicate that MinE containing the D45A or D45A/V49A mutations is deficient in overcoming the inhibitory activity of MinC/MinD. To investigate the basis for this deficiency we purified MinE-6xHis and MinE$^{D45A/V49A}$-6xHis to test the interaction with MinD. In the presence of ATP, MinD recruits MalE-MinC to lipid vesicles (4, 5). The addition of MinE to the reaction displaces MalE-MinC and stimulates the MinD ATPase releasing MinD from the membrane. MinE$^{D45A/V49A}$, in contrast, was unable to remove MalE-MinC or MinD from the vesicles (Fig. 3*A*), indicating that the double mutant (DM) was defective in competing with MalE-MinC for overlapping binding sites located at the dimeric interface of MinD. To test directly whether interaction between MinD and MinE is compromised

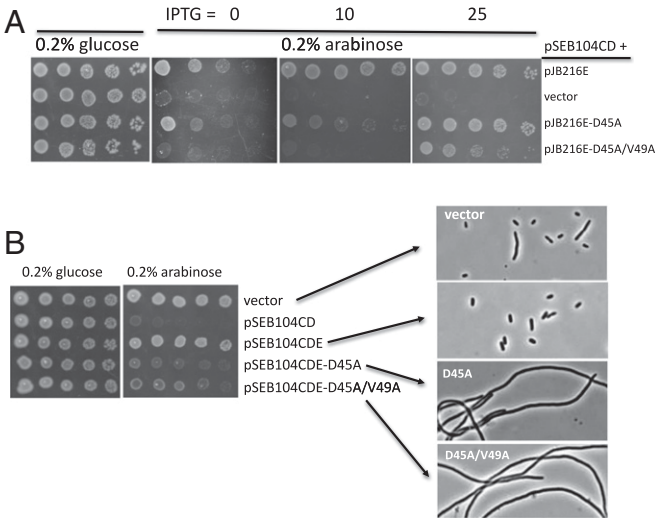

Fig. 2. MinE^{D45A} and MinE$^{D45A/V49A}$ mutants have reduced activity. (*A*) The effect of expression of MinE^{D45A} and MinE$^{D45A/V49A}$ on suppression of MinC/MinD in *trans*. pSEB104CD (P$_{BAD}$::*minC minD*) and pJB216E (P$_{lac}$::*minE*) or variants containing *minE^{D45A}* or *minE$^{D45A/V49A}$*, or the vector (pUC18), were introduced into JS964 (Δ*min*) and grown on LB plates containing ampicillin, spectinomycin, and 0.2% glucose. A colony of each strain was resuspended and serially diluted 10-fold and 3 μL of each dilution was spotted on plates containing glucose or arabinose with increasing IPTG. (*B*) MinE^{D45A} and MinE$^{D45A/V49A}$ are defective in counteracting MinC/MinD in *cis*. Plasmid pSEB104CDE (P$_{BAD}$::*minC minD minE*) and variants containing *minE^{D45A}* or *minE$^{D45A/V49A}$* were transformed into JS964 (Δ*min*) and selected on LB plates containing spectinomycin and 0.2% glucose. Colonies were picked and spot-tested as described in *A*. Some of the strains in *B* were grown to exponential phase in liquid culture and photographed 3 h after the addition of 0.2% arabinose.

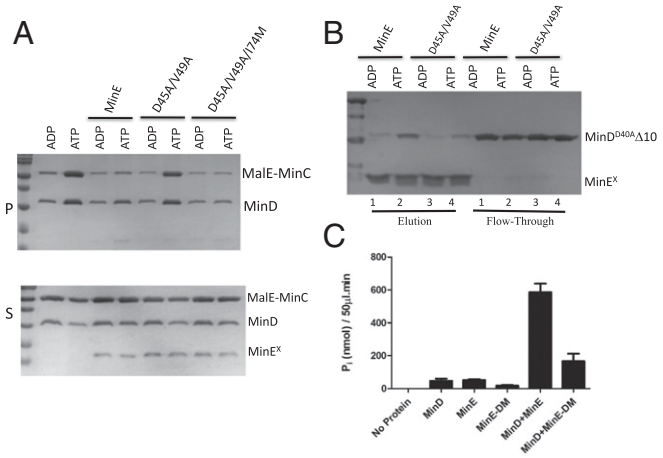

Fig. 3. MinE$^{D45A/V49A}$ is deficient in interaction with MinD in vitro. (*A*) MinE$^{D45A/V49A}$ fails to displace MinC and MinD from lipid vesicles. MinD, MalE-MinC, and MinE and MinE$^{D45A/V49A}$ or MinE$^{D45A/V49A/I74M}$ were incubated with phospholipid vesicles in the presence of ADP or ATP. The vesicles were collected by centrifugation and the bound proteins (P = pellet) as well as the supernatants (S) were analyzed by SDS/PAGE. (*B*) MinE$^{D45A/V49A}$ exhibits reduced binding to MinD. MinD^{D40A}Δ10 was incubated with MinE-6xHis or MinE$^{D45A/V49A}$-6xHis in the presence of ADP or ATP. The samples were loaded on a Ni-NTA column to allow MinE-6xHis or MinE$^{D45A/V49A}$-6xHis to attach to the column matrix. Bound proteins were eluted with imidazole and samples run on SDS/PAGE. (*C*) MinE$^{D45A/V49A}$ poorly stimulates MinD's ATPase activity. MinD and MinE or MinE$^{D45A/V49A}$ (indicated as MinE-DM) were mixed with lipid vesicles in the presence of ATP and phosphate released was measured.

we purified MinD^{D40A}Δ10, a MinD catalytic mutant lacking its C-terminal MTS. As shown previously (16), this protein can be used for testing direct interaction with MinE because it lacks ATPase activity, thereby retaining bound MinE. In vitro pull-down experiments revealed that the binding of MinE$^{D45A/V49A}$ to MinD^{D40A}Δ10 was significantly diminished compared with MinE (Fig. 3*B*).

Our findings suggest that the aberrant Min oscillation observed in the presence of MinE$^{D45A/V49A}$ is primarily due to weak interaction between MinE$^{D45A/49A}$ and MinD. However, it was previously reported that activation of the MinD ATPase by MinE$^{D45A/V49A}$ is similar to that by MinE (22). The result is rather puzzling, because in the same study it was shown that MinE$^{D45A/V49A}$ exhibited diminished binding to MinD in a bacterial two-hybrid assay. Hence, to resolve the conundrum we examined the ability of MinE$^{D45A/V49A}$ to activate the MinD ATPase. Consistent with our binding studies, MinE$^{D45A/V49A}$ was significantly impaired in stimulating MinD's ATPase activity (Fig. 3*C*).

HDX Reveals a Stable Core and Unveils Differences in Conformational Dynamics Between MinE and MinE$^{D45A/V49A}$. The structure of MinE from *Neisseria gonorrhoeae* (*Ng*MinE) was determined by NMR spectroscopy (18). Interestingly, *Ng*MinE^{E46A}, the equivalent of *Ec*MinE^{D45A}, was used for the structural determination, because it displayed more favorable solubility characteristics than WT *Ng*MinE. Nonetheless, circular dichroism and backbone NMR secondary chemical shifts did not reveal any notable differences between *Ng*MinE and *Ng*MinE^{E46A}. We suspected that the mutation improves the solubility by making it more difficult for MinE to release the MTS, avoiding aggregation. To gain insight into the structural dynamics of MinE and possible differences between MinE and MinE$^{D45A/V49A}$ we used HDX-MS, because this technique can detect protein conformations and dynamics in solution.

MinE and MinE$^{D45A/V49A}$ were diluted 10-fold into a neutral-pH deuterated buffer for initiation of the HDX reaction (final protein concentration of 5 μM, in 90% D_2O). At different time points samples were removed and subjected to pepsin digestion and MS analysis (details are described in *Materials and Methods*). Monitoring deuterium content as a function of time showed that most secondary structural elements of both MinE and MinE$^{D45A/V49A}$ could take up deuterium (Fig. 4 and Fig. S1). Importantly, following data consolidation analysis (23), central residues in the β1 strand and in the coiled coil, including the D45/V49 tetrad that packs against the β1 strand, did not undergo HDX in either protein (Fig. 4). This result indicates that the β1 strand is tightly packed against the coiled coil and is not exposed to solvent during extended incubation. The central regions of the β1 strand and the coiled coil did not undergo exchange, which indicates the 4β and 6β forms of MinE do not spontaneously interconvert, ruling out an equilibrium model.

The mass spectra indicated that most regions of the two proteins display EX2 kinetic signatures characterized by rapid monophasic increases in average mass. However, a region of the protein (peptide ^{7}FLSRKNTANIAKERL^{22}) in the N-terminal region of MinE$^{D45A/V49A}$ underwent EX1 exchange kinetics,

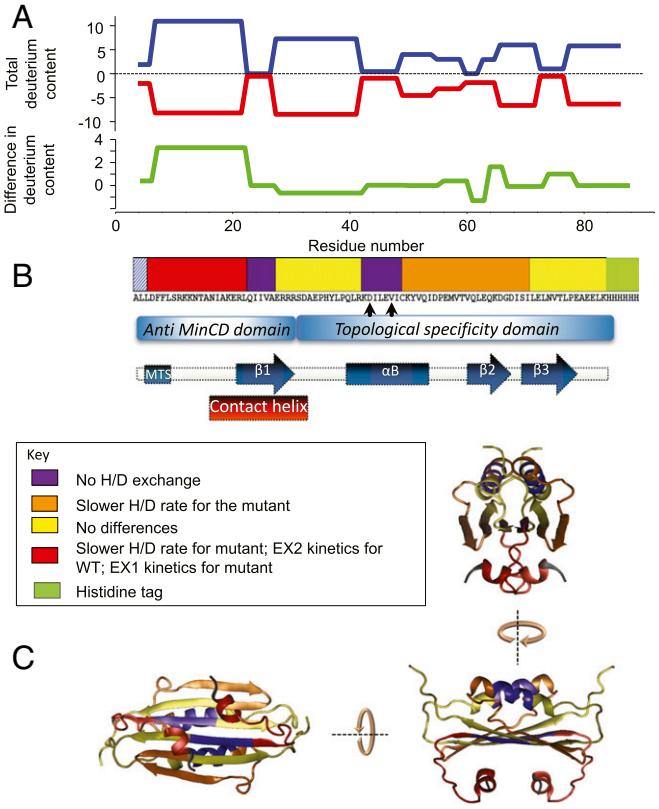

Fig. 4. HDX-MS analysis of MinE and MinE$^{D45A/V49A}$. (*A*) Butterfly plot summarizing the analysis of deuterium content in peptides obtained following pepsin digestion of MinE at different time points following the initiation of the HDX reaction. Total deuterium uptake for each peptide (repeated twice) at the end of the 2 h of exchange (Fig. S1 and Table S1) is summarized in the butterfly plot. The blue line is for the WT protein and the red line is for the D45A/V49A (DM) protein. The green line represents the difference in total deuterium uptake of the WT protein relative to the DM. (*B*) Summary of the deuterium uptake and the secondary structure of MinE. The colored bar (see key) illustrates the relative position of the main differences in deuterium uptake between the two proteins. (*C*) Exchange indicated on the 3D structure of MinE. The cartoon diagrams were generated using the program VMD (Theoretical Biophysics Group, University of Illinois at Urbana–Champaign) and the NMR structure of MinE (PDB ID code 2KXO) from *N. gonorrhoeae*. The color coding indicates differences in either total deuterium content or in the rates of exchange as indicated in the Key.

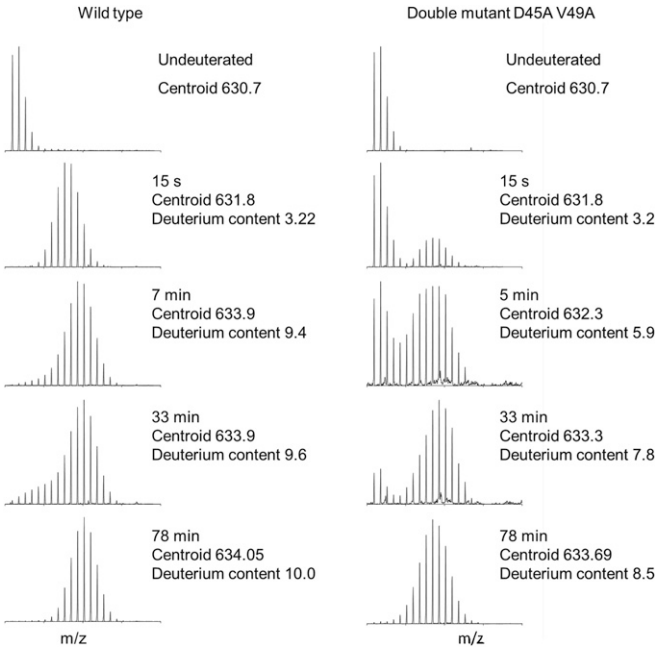

Fig. 5. Kinetics of deuterium labeling of a peptide corresponding to the loop region of MinE. Representative isotope peptide profiles at different times of HDX of the triply charged peptide (^{7}FLSRKNTANIAKERL^{22}) originating from the loop region of the WT protein undergoes EX2 kinetics, whereas the same peptide from the DM undergoes EX1 kinetics.

yielding two distinct mass envelopes (Fig. 5). This peptide forms a loop that connects the MTS to the β1 strand (Fig. 1). During the first minute of the HDX reaction, 82% of the exchangeable protons of MinE and 60% of those of MinE$^{D45A/V49A}$ were rapidly labeled. The second rate was significantly slower for MinE$^{D45A/V49A}$ than for MinE (Fig. S1). This result indicates this peptide in the D45A/V49A mutant undergoes a slow, cooperative unfolding event wherein a number of residues in this region are simultaneously exposed to solvent and labeled. In contrast, in the WT protein this peptide is more rapidly labeled with EX1 kinetics, suggesting that it has multiple dynamic conformations (Fig. 5). Overall, our results indicate that MinE$^{D45A/V49A}$ is in a more rigid conformation than the WT protein and may have difficulty in releasing the MTS. This would be consistent with its having difficulty in switching to the active conformation.

Isolation of an Intragenic Suppressor of MinE$^{D45A/V49A}$. As indicated above JS964/pSEB104CDE-D45A/V49A and JS964/pSEB104CDE-D45A did not grow on LB plates containing 0.2% arabinose; however, suppressors arose spontaneously. Although most suppressors are likely due to mutations in *minC* or *minD*, it is possible that intragenic suppressors that restore MinE activity might also be present. Understanding intragenic suppressors should give further insight into the MinE activation mechanism. As expected most suppressors contained mutations in *minC* or *minD*; however, we identified one intragenic suppressor of JS964/pSEB104CDE-D45A/V49A, *minE^{I74M}*, which rescued MinE$^{D45A/V49A}$ (Fig. 6*A*). It also rescued MinE^{D45A}.

The I74 residue is located in β3 and is involved in tethering the MTS to the six-stranded β-sheet (18) (Fig. 1). If tethering the MTS to the 6β-sheet is weakened by mutations like I74M, then the I74M mutant might bind to the membrane in the absence of MinD. Whereas MinE-GFP is located in the cytoplasm, MinE^{I74M}-GFP is constitutively localized on the membrane, confirming that the MTS is released (Fig. 6*B*). Consistent with this, Zheng et al. (24) found several substitutions at the I74 position (I74A and I74R) that also caused constitutive membrane binding. Together, these results demonstrate the I74 is a critical residue for tethering the MTS to the β-sheet and that even substitutions resulting in methionine or alanine disrupt this tethering function.

Previously, we showed that mutations that disrupt the 6β-stranded structure of MinE lead to constitutive membrane binding (16). Because the I74M is a relatively conservative substitution it would not be expected to disrupt the 6β-stranded structure. To check this, we examined the ability of MinE$^{21–88/I74M}$ to form 6β-stranded heterodimers with WT MinE. Previously, we showed that a truncated MinE (lacking the MTS and loop region) is dominant-negative because it forms 6β-stranded heterodimers with WT MinE that are unable to protect cells from the inhibitory activity of MinC/MinD (16). In contrast, such a truncated MinE was unable to inhibit mutants such as MinE^{I24N}, which are locked in the 4β-stranded conformation (16). As shown in Fig. 5*C*, expression of MinE$^{21–88/I74M}$ inhibits the growth of JS964/pSEB104CDE as efficiently as MinE$^{21–88}$, indicating the I74M mutation does not affect the ability of the truncated MinE to form 6β-stranded heterodimers with WT MinE. We also tested MinE$^{21–88/I74R}$ and found that it is slightly less effective at inhibiting the growth of JS964/pSEB104CDE. Thus, we conclude that the I74M mutation does not affect the 6β-stranded structure, whereas I74R probably reduces the fraction of MinE that is in the 6β-stranded form.

So far the results indicate that the I74M mutation causes the release of the MTS without affecting the structure of the 6β-stranded sheet. If so, the phenotype of cells expressing I74M would not be WT due to its constitutive membrane binding. Although a MinE mutant that is constitutively on the membrane can suppress the inhibitory effect of MinC/MinD, it cannot support the Min oscillation (16, 24). As expected, JS964/pSEB104CDE-I74M displayed a minicell phenotype when grown with 0.2% arabinose (Fig. 6*D*).

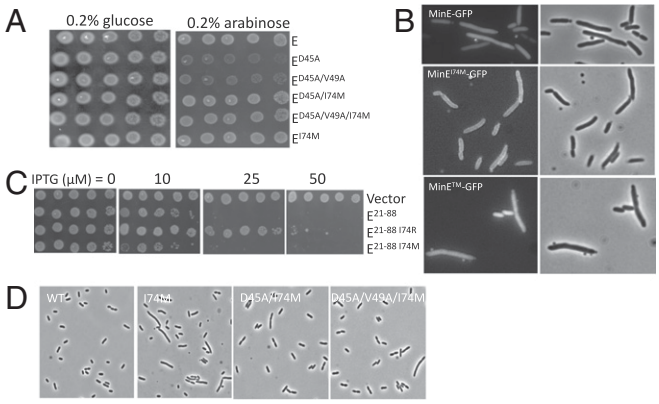

Fig. 6. The *minE$^{D45A/V49A}$* and *minE^{D45A}* mutations are suppressed by the intragenic I74M mutation in vivo. (*A*) The I74M mutation suppresses the growth defect of the D45A/V49A and D45A mutations in *cis*. pSEB104CDE (P$_{BAD}$::*minC minD minE*) and variants containing *minE^{D45A}*, *minE$^{D45A/49A}$*, *minE$^{D45A/I24N}$*, *minE$^{D45A/V49A/I24N}$*, or *minE^{I74M}* were introduced into JS964 (Δ*min*) and spot-tested as in Fig. 2. (*B*) The I74M mutation causes constitutive membrane binding. JS964 (Δ*min*) containing plasmids expressing MinE-GFP, MinE^{I74M}-GFP, or MinE$^{D45A/V49A/I74M}$-GFP (MinE^{TM}-GFP) were analyzed by fluorescence microscopy. (*C*) The I74M mutation does not affect the ability of MinE$^{21–88}$ to inhibit MinE in *trans*. JS964 containing JS964 (Δ*min*)/pSEB104CDE (P$_{BAD}$::*minC minD minE*) was transformed with derivative of pJB216E (P$_{lac}$::*minE*) variants containing *minE$^{21–88}$*, *minE$^{21–88/I74R}$*, or *minE$^{21–88/I74M}$* and spot-tested as in Fig. 2. Note that MinE$^{21–88/I74M}$ inhibits as well as MinE$^{21–88}$. (*D*) Effect of I74M on cell morphology. JS964 (Δ*min*) containing pSEB104CDE (P$_{BAD}$::*minC minD minE*) or variants containing *minE^{I74M}*, *minE$^{D45A/I74M}$*, or *minE$^{D45A/V49A/I74M}$* were grown to exponential phase in LB with 0.2% arabinose and samples examined by phase contrast microscopy.

The presence of I74M in the D45A/V49A background presumably also favors the release of the MTS and this counteracts the rigidity caused by the D45A/V49A mutations. To check this, we examined the localization of MinE$^{D45A/V49A/I74M}$. In contrast to MinE^{I74M}-GFP, which is on the membrane, the triple mutant (TM), just as the WT, is in the cytoplasm in the absence of MinD (Fig. 6*B*, *Bottom*). Interestingly, the triple mutant, like the WT, also had the ability to displace MinC and MinD from vesicles in vitro (Fig. 3*A*). Together, these results argue that MinE$^{D45A/V49A}$ has difficulty in releasing the MTS, which is counteracted by weakening the MTS tether with the I74M substitution.

To see to what extent the I74M restored activity to the D45A/V49A mutant, we checked the cell morphology of the triple mutant D45A/V49A/I74M. Whereas JS964/pSEB104CDE-D45A/V49A had a filamentous morphology (Fig. 2*B*), JS964/pSEB104CDE-D45A/V49A/I74M, as well as JS964/pSEB104CDE-D45A/I74M, displayed a more homogeneous cell length distribution with few minicells present (Fig. 6*D*). Together, our results indicate that I74M is an intragenic suppressor of D45/V49A, indicating that weakening the tether of the MTS compensates for the rigidity caused by the D45A/V49A mutations. These results argue that the first step in the transition from the 6β- to the 4β-stranded structure is the release of the MTS. Presumably, releasing the MTS frees the loop region, which contains residues that contribute to MinD binding, allowing the loop region to sense MinD.

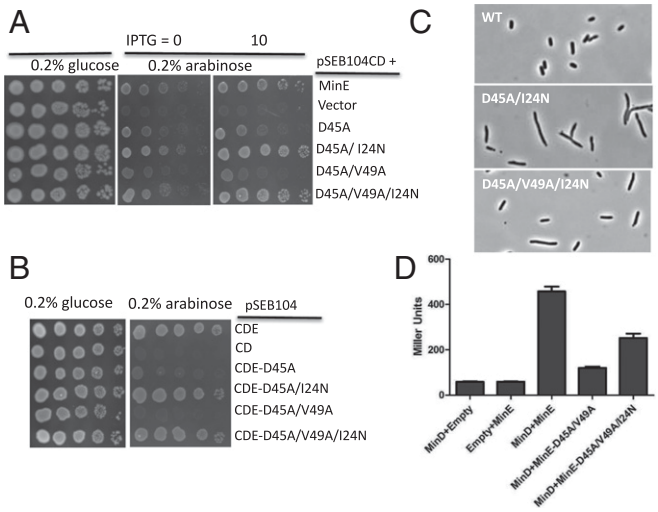

Fig. 7. The *minE*$^{D45A/V49A}$ and *minE*^{D45A} mutations are suppressed by an intragenic I24N mutation in vivo. (*A*) MinE$^{D45A/V49A/I24N}$ counters the inhibitory activity of MinC/MinD in *trans*. pSEB104CD (*P*$_{BAD}$::*minC minD*) and pJB216E (P$_{lac}$::*minE*) or variant s containing *minE*^{D45A}, *minE*$^{D45A/I24N}$, *minE*$^{D45A/I49A}$, or *minE*$^{D45A/V49A/I24N}$ were introduced into JS964 (Δ*min*). A colony was picked from glucose plates into LB, serially diluted, and spotted on plates containing various IPTG concentrations and 0.2% arabinose as in Fig. 2. (*B*) The *minE*^{I24N} mutation suppresses *minE*^{D45A} and *minE*$^{D45A/V49A}$ for colony formation in *cis*. pSEB104CDE (P$_{BAD}$::*minC minD minE*) and variants containing *minE*^{D45A}, *minE*$^{D45A/I24N}$, *minE*$^{D45A/V49A}$, or *minE*$^{D45A/V49A/I24N}$ were transformed into JS964 (Δ*min*). Cells containing the plasmids were grown overnight on glucose plates with spectinomycin. A spot test was conducted as described in Fig. 2*A*. (*C*) Cells expressing MinE$^{D45A/V49A/I24N}$ or MinE$^{D45A/I24N}$ along with MinC/MinD display a minicell phenotype. JS964 with pSEB104CDE (*P*$_{BAD}$::*minC minD minE*) and variants containing *minE*$^{D45A/V49A}$ or *minE*$^{D45A/V49A/I24N}$ were cultured to exponential phase in LB containing 0.2% arabinose before photography. (*D*) Bacterial two-hybrid test reveals the intragenic I24N suppressor mutation suppresses the interaction defect of MinE$^{D45A/V49A}$ with MinD. BTH101 (Δ*min*) was transformed with pCT25-MinD and pUT18-MinE, pUT18 MinE-D45A/V49A, or pUT18 MinE-D45A/V49A/I24N. Cells were grown on glucose plates containing ampicillin and chloramphenicol. Protein expression was induced with 0.5 mM IPTG at 30 °C and β-galactosidase activity of each strain was quantitated using a colorimetric assay.

MinE^{I24N} Is an Intragenic Suppressor of Some MinE$^{D45A/V49A}$ Defects. The I24 residue is located in the middle of the β1 strand and contributes to the hydrophobic interior of MinE, packing against hydrophobic residues from the coiled coil (Fig. 1). In a previous study we demonstrated that hydrophilic substitutions at this position, such as I24N, lock MinE in a 4β-stranded conformation whereas a hydrophobic substitution (I to V) did not (16). Also, such substitutions have little impact on MinD binding because the I24 residue resides on the opposite face of the contact helix bound to MinD (16). Although such substitutions do not restore the oscillation (the I24N mutant is constitutively on the membrane), they do suppress the inhibitory activity of MinC/MinD, allowing cells to grow. If MinE$^{D45A/V49A}$ is impaired in the activation step due to structural rigidity preventing the release of the MTS, the I24N mutation would be expected to restore the ability of Min$^{D45A/V49A}$ to suppress MinC/MinD inhibition by forcing it into the active form.

To check this, pSEB104CD (P$_{BAD}$::*minC minD*) and pJB216E (P$_{lac}$::*minE*) or variants encoding *minE*$^{D45A/I24N}$ or *minE*$^{D45A/V49A/I24N}$ were cotransformed into JS964 (Δ*min*). On LB plates containing only arabinose (i.e., in the absence of IPTG) the basal expression of these mutants partially overcame the inhibitory activity of MinC/MinD (Fig. 7*A*); however, the rescue was complete at 10 μM IPTG. To see the effect of the I24N mutation at the physiological level we introduced pSEB104CDE (P$_{BAD}$::*minC minD minE*) or variants carrying *minE*$^{D45A/I24N}$ or *minE*$^{D45A/V49A/I24N}$ into JS964. Spot tests of single colonies revealed that the I24N mutation suppressed both *minE*^{D45A} and *minE*$^{D45A/V49A}$ in *cis* (Fig. 7*B*).

Because addition of the I24N mutation to *minE*$^{D45A/V49A}$ and *minE*^{D45A} rescued colony formation in *cis*, the phenotype of the cells expressing MinC/MinD with either MinE$^{D45A/V49A}$ or MinE$^{D45A/V49A/I24N}$ was examined. As described above, both JS964/pSEB104CDE-D45A and JS964/pSEB104CDE-D45A/V49A exhibited extensive filamentation in LB medium containing arabinose, whereas JS964/pSEB104CDE exhibited a WT morphology (Figs. 2*B* and 7*C*). The addition of the *minE*^{I24N} mutation to either of these MinE mutants suppressed filamentation and resulted in a minicell phenotype (Fig. 7*C*, *Middle*). This is unlike the addition of the I74M mutation, which resulted in a morphology with few minicells (Fig. 6*D*). Because the I24N mutation suppressed the deficiency of *minE*^{D45A} and *minE*$^{D45A/V49A}$ in counteracting MinC/MinD in vivo, it likely restores interaction with MinD. To corroborate this, we used a bacterial adenylate cyclase two-hybrid system and a quantitative β-galactosidase assay (25). The interaction of MinE$^{D45A/V49A}$ with MinD was weak, consistent with the weak stimulation of the MinD ATPase (Fig. 3*C*). The addition of the I24N mutation to MinE$^{D45A/V49A}$ resulted in a more than twofold increase in the interaction with MinD so that it was over 50% of the WT activity (Fig. 7*D*). This result is consistent with the hypothesis the I24N mutation is an intragenic suppressor of the D45A/V49A mutation.

Comparison of the Suppression of MinD^{M193L} by MinE^{I74M} and MinE^{I24N}. As shown above MinE^{I74M} binds constitutively to the membrane in vivo, indicating that this substitution favors release of the MTS. In addition, the I74M mutation suppresses the D45A/V49A mutant, indicating it counteracts the rigidity of this mutant to allow it to bind MinD and behave like a WT protein. Together, these results suggest that the deficiency of the D45A/V49A mutant is the ability to release the MTS and free up the loop region to contact MinD (sensing step) so that the subsequent step in the activation pathway can occur.

Previously, we reported that MinD^{M193L} does not respond to MinE (14). Our explanation was that it is unable to sense MinE and therefore trigger the release of the β1 strand. However, MinD^{M193L} responds to MinE^{I24N} because the I24N mutation forces MinE into the 4β-stranded conformation and the sensing

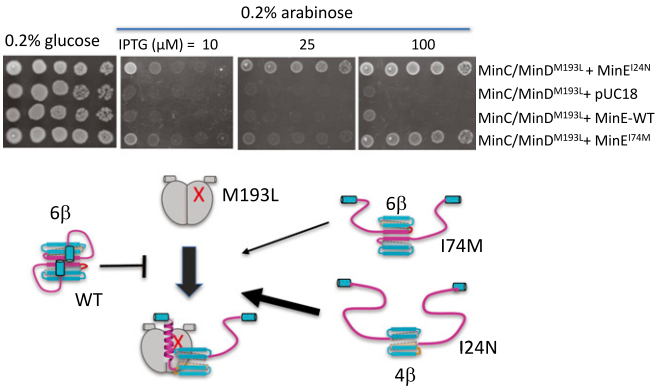

Fig. 8. Suppression of MinC/MinD^{M193L} by MinE mutants. JS964 (Δ*min*)/pSEB104CD (P_{BAD}::*minC minD*^{M193L}) was transformed with pJB216E (P_{lac}::*minE*) or variants containing *minE*^{I24N} or *minE*^{I74M}. A single colony of each transformant was picked into LB, serially diluted, and spotted on plates containing 0.2% glucose or 0.2% arabinose and increasing concentrations of IPTG. The diagram indicates the structure of WT MinE and the two mutants, I74M and I24N, and their ability to interact with MinD^{M193L}.

step is bypassed since the β1 strand is already released (Fig. 8). Therefore, if MinD^{M193L} is deficient in sensing it should not be easily suppressed by MinE^{I74M} because the sensing step is not bypassed. This is what was observed. Fig. 8 shows that MinE^{I74M} was much less efficient than MinE^{I24N} in combating the inhibitory activity of MinD^{M193L}/MinC. Even though I74M restored the growth of a strain expressing MinD^{M193L}/MinC at high IPTG concentrations, the cell morphology was extremely filamentous. In contrast, with I24N the cell morphology was Min^{-}. Thus, MinE^{I24N} is much more effective in overcoming the MinD^{M193L} deficiency than MinE^{I74M}, as summarized in the diagram in Fig. 8.

Discussion

In our previous study (16) we showed that MinE can exist in two conformations, latent (6β) and active (4β); however, it was not clear how MinE transitions between these conformations. At least two models were possible. In one, the two conformations are in equilibrium and the equilibrium is pulled toward the active 4β conformation by binding to MinD. In the other, MinD is directly involved in the transition by inducing the switch. We favored the second possibility and proposed a "sensing model" in which MinE is induced to switch upon contact with MinD (16). Here we provide additional support for the sensing model and propose that in the 6β-stranded conformation the MTS is dynamically associated with the β-sheet, resulting in the closed and open states (Fig. 9*A*). We propose that in the open state (MTS released) MinE residues in the loop region contact MinD (sensing step), which nucleates formation of the contact helix. Once nucleated the helix propagates into the β1 strand, inducing the final step in the transition from the latent to the active form (Fig. 9*A*).

Importantly, the absence of HDX in the central regions of β1 and the coiled coil in contact with β1 of the WT protein indicates that MinE does not undergo a spontaneous release of β1. This result rules out a model in which the two forms are in equilibrium and is consistent with the observation that MinE remains a dimer during the transition from the latent to the active form; the coiled coil must act as a hinge holding the MinE dimer together during the transition (26). Ruling out the equilibrium model raises the question about how the transition is achieved and what the pathway is.

The analysis of the MinE$^{D45A/V49A}$ mutant revealed that it is deficient in interaction with MinD: (*i*) reduced binding, (*ii*) poor stimulation of the MinD ATPase, and (*iii*) inability to compete with MinC for binding to MinD. The HDX-MS analysis indicated that it is more rigid than the WT, with the major differences in deuterium exchange occurring in residues in the loop region connecting the MTS to the β1 strand (Fig. 1). The peptides corresponding to this region exchange hydrogen atoms for deuterium atoms with EX2 kinetics whereas the mutant exchanges with EX1 kinetics (Fig. 5). EX2 kinetics implies multiple dynamic conformations, whereas EX1 kinetics indicate that this region undergoes a cooperative unfolding event in which all residues are exchanged almost simultaneously. Because this unfolding step is slow in the mutant MinE, it suggests that MinE in the closed state is unable to interact with MinD.

Two suppressors of MinE$^{D45A/V49A}$ were studied in detail, I74M and I24N, with I74M being more informative. On its own the I74M mutation causes release of the MTS and constitutive membrane binding without affecting the structure of the six stranded β-sheet. Interestingly, combining the I74M mutation with the D45A/V49A mutations yielded a *minE* with behavior intermediate between the separate mutants. In the presence of MinC/MinD, I74M produced a minicell phenotype and D45A/V49A resulted in filamentation, whereas the triple mutant resulted in more a homogeneous population with few minicells. The ability of these mutations to compensate for each other is also indicated by interaction with the membrane in the absence of MinD; whereas the I74M mutant is constitutively on the membrane the triple mutant, like the WT protein, is in the cytoplasm.

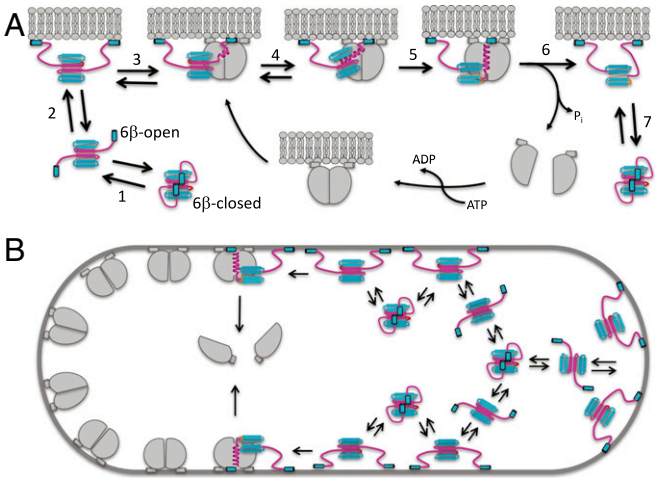

Fig. 9. Models for MinD's role in the activation of MinE and a role for MinE's dynamic association with the membrane in MinE ring formation. (*A*) Activation of MinE. The 6β-stranded form of MinE exists in two conformations, closed and open. Switching between these two forms is very dynamic (16) (step 1). For MinE$^{D45A/V49A}$ this step is significantly compromised due to the rigidity of the structure but is suppressed by the I74M mutation, which weakens the association of the MTS. The open form interacts reversibly with the membrane (step 2). If the loop region encounters MinD it converts to a nascent α helix (step 3). The nucleation of the nascent helix on MinD stimulates a propagation of the α helix into the β1 strand, inducing its dissociation from the dimer interface (step 4). The α helix (contact helix) is then stabilized by binding to the dimeric interface of MinD to form a complex (step 5), which results in stimulation of the MinD ATPase and the release of MinD (step 6). If the MinE does not encounter another MinD it spontaneously returns to the latent form (step 7). (*B*) A role for the dynamic association of MinE with the membrane in forming a MinE ring. This diagram represents a snapshot in the oscillation. A MinE ring processively removes MinD as it moves to the right pole. The released MinD has formed a new polar zone at the opposite pole. As MinE is released from the right pole it dynamically associates with the membrane, causing it to diffuse close to the membrane scanning for MinD. Once it encounters the edge of the MinD polar zone it converts to the active form and stimulates the MinD ATPase, which is the rate-limiting step in this process, causing MinE to accumulate into a ring. Some MinE is also associated with MinD in the polar zone and is not indicated here.

Also, I74M rescues the ability of the D45A/V49A mutant to displace MinC/MinD from membrane vesicles in vitro. Together, these results indicate that the D45A/V49A deficiency is overcome by weakening the MTS tether with the I74M mutation. Although the I24N mutation also suppresses the DM's reduced ability to counteract MinC/MinD, this is not surprising because this mutation releases both the MTS and β1 as it forces MinE into the active 4β-strand conformation.

Also informative is the effect of the *minE* mutations in suppressing $MinD^{M193L}$, which cannot be suppressed by overexpression of WT MinE. Previously, it was shown that this MinD mutant has a deficiency in interacting with MinE, but not MinC (14). However, forcing the release of the MTS and the β1 strand by the I24N mutation allows suppression of $MinD^{M193L}$, whereas releasing just the MTS with the I74M mutation does not. The I24N mutation causes MinE to be constitutively in the 4β active form, allowing $MinD^{M193L}$ to bind the released β1, bypassing the sensing step. In contrast, although I74M releases the MTS and causes constitutive membrane binding, it is in the 6β form and the sensing step is still required to flip the switch to the active form, something $MinD^{M193L}$ cannot provide.

In vitro work examining MinE-MinD pattern formation on a lipid bilayer indicates that MinE lacking the MTS reacts as fast or faster with MinD than the WT protein (27). Such a mutant is more effective in supporting a wave pattern in vitro, but it is unable to produce bursts (radial regions of MinD surrounded by MinE), which are thought to most closely resemble the in vivo oscillation. This ability of MinE lacking the MTS to interact with MinD argues that tethering the MTS to the β-sheet is not necessary for MinD interaction but in fact impedes it. Analysis of substitutions at residue E66 argue that a strong tether inhibits the interaction with MinD. An E66A mutation in *E. coli minE* has no effect on activity, whereas changing the equivalent residue in *N. gonorrhoeae* MinE to a large hydrophobic residue (E67L) resulted in a dramatic loss of activity (19, 28). This glutamate is in the β2 strand oriented toward the MTS (Fig. 1). It is likely that replacing a charged residue with a large hydrophobic residue strengthens the tethering of the MTS to the β-sheet, making it more difficult for it to be released, behaving similarly to the D45A/V49A mutant.

Together the results lead to the following model for the activation of MinE. MinE in the cytoplasm has the MTS dynamically tethered to the β-sheet (Fig. 9*A*, step 1), which leads to reversible interaction with the membrane (Fig. 9*A*, step 2). Dynamic tethering of the MTS to the β-sheet is supported by NMR analysis (16). When the MTS is released the loop region is available to interact with MinD. Because MinD dimers are bound to the membrane, we assume these steps occur at the membrane. As residues in the loop region contact MinD, formation of the contact helix is nucleated, which propagates into β1, causing it to be released from the dimer interface producing the active 4β strand conformation (Fig. 9*A*, steps 3–5). Once the MinD ATPase is stimulated (Fig. 9*A*, step 6), MinD is released from the membrane and MinE can linger at the membrane in the 4β conformation. If it does not encounter another MinD, it spontaneously returns to the latent 6β-stranded form (Fig. 9*A*, step 7).

This study highlights the importance of the strength of the tether of the MTS to the β-sheet. Mutations that weaken this association result in a MinE that is constitutively on the membrane but in the 6β-strand conformation in the absence of MinD. Thus, binding to the membrane does not trigger the 6β- to 4β-strand switch. In contrast, mutations that make the tether stronger or make the protein more rigid so the MTS is less dynamic lead to a MinE that is in the cytoplasm with reduced ability to interact with MinD. It is not clear why the D45A/V49A mutant is more rigid and therefore has difficulty in reaching the open state (released MTS). Inspection of the MinE structure suggests that these substitutions may lead to tighter packing of the coiled coil, which may reduce the flexibility of MinE. It is clear, however, that mutations like I74M, which weakens the association of the MTS, rescue the activity of such a rigid mutant.

In summary, the MinE structure has evolved a delicate balance so that it can carry out two distinct functions; act at the membrane to remove MinD and diffuse in the cytoplasm. To do this, MinE has evolved so that the MTS is dynamically tethered to the six-stranded β-sheet so that MinE spends enough time in the open state to give it a chance to sense MinD but not so long that it will get trapped on the membrane and be unable to diffuse in the cytoplasm, which is required to produce the oscillation. We also propose that this dynamic tethering of the MTS contributes to the formation of the MinE ring (Fig. 9*B*). During the oscillation cycle, the MinE ring processively removes MinD from a polar zone. The released MinD forms a new polar zone at the opposite pole that extends toward midcell. Eventually, the MinE is also released from the pole (Fig. 9*B*, right pole) and because of its ability to dynamically associate with the membrane it scans the membrane for the presence of MinD (Fig. 9*B*). MinE that encounters the edge of the MinD polar zone converts to the active form and stimulates the MinD ATPase. Because this step is slow it acts as a trap, causing MinE to accumulate in a ring. Some MinE escapes this trap and enters the polar zone. It has also been suggested that MinE dimers interact through the released β1 strands to form oligomers that contribute to MinE ring formation (25). Although it is possible that such interactions contribute to MinE ring formation, it may not be necessary.

Materials and Methods

Strains and Media. The *E. coli* K12 strain JS964 (*MC1061 malP::lacI^q minB::kan*) was used for cell division inhibition by MinC/MinD and Min phenotype complementation by MinC/MinD/MinE (16). Most plasmid constructions and protein purifications were carried out using JS964 strain. BTH101 Δ*min* strain [F$^-$*cya*-99, *ara*D139, *gal*E15, *gal*K16, *rps*L1 (Str^r), *hsd*R2, *mcr*A1, *mcr*B1] with its *minB* operon deleted and replaced with a kan-resistance cassette was used for β−galactosidase assay (14). Unless stated otherwise, LB medium containing 0.5% NaCl was used and antibiotics (100 μg/mL ampicillin and 50 μg/mL spectinomycin), IPTG, glucose (0.2%), or arabinose (0.2%) were added accordingly.

Plasmids. Plasmids pSEB104CD (P_{BAD}::*minC minD*), pSEB104CDE (P_{BAD}::*minC minD minE*), and pJB216E (P_{lac}::*minE*) were described previously (21). The $minE^{D45A}$ and $minE^{D45A/V49A}$ mutations were introduced into pSEB104CDE and pJB216E using the QuikChange II kit according to the manufacturer's instructions (Agilent Technologies). The construction of pCT25 (Cm^R), a derivative of pKT25, and pUT18 was described before (14). To construct pCT25-MinD (cya^{T25}-*minD*), *minD* was PCR-amplified, digested with BamHI/KpnI, and ligated into linearized pCT25 (cya^{T25}). pUT18-MinE (cya^{T18}-*minE*) was generated by PCR amplification of *minE* followed by digestion with BamHI/KpnI and ligation into the corresponding sites of pUT18 vector (cya^{T18}).

Protein Expression and Purification. The purification of MinD and $MinD^{D40A}$ Δ10 were previously described (14). MinE-6xHis and $MinE^{D45A/V49A}$-6xHis were purified from JS964 (Δ*min*) containing pJB216Eh (*minE-6xhis*) and its variant pJB216E-D45A/V49Ah ($minE^{D45A/V49A}$-*6xHis*) as described previously (16). JS964/pJB216Eh was cultured at 37 °C and IPTG (1 mM) was added at OD_{600} ~0.5. After 3 h of induction, cells were harvested and stored at −80 °C until processed. The cell pellet was thawed, resuspended in lysis buffer (25 mM Tris·HCl, pH 7.9, 100 mM NaCl, 10 mM imidazole, and 10% glycerol), and lysed with a French press. The lysates were centrifuged at 10,000 × *g* at 4 °C for 30 min and supernatants were applied to nickel-agarose column equilibrated with the lysis buffer. The column was washed with washing buffer (25 mM Tris·HCl, pH 7.9, 500 mM NaCl, 20 mM imidazole, and 0.1% Nonidet P-40) and MinE-6xHis and $MinE^{D45A/V49A}$-6xHis were eluted with elution buffer (25 mM Tris·HCl, pH 7.9, 500 mM NaCl, and 250 mM imidazole). The eluted fractions were pooled together and dialyzed with dialysis buffer (25 mM Hepes-NaOH, pH 7.0, 250 mM NaCl, 1 mM EDTA, and 10% glycerol) and aliquots stored at −80 °C.

Vesicle Binding and Pull-Down Assay. MinD, MalE-MinC, and MinE-6xHis (or $MinE^{D45A/V49A}$-6xHis) were incubated for 10 min at 25 °C in the presence of ADP or ATP (1 mM) and multilamellar vesicles (MLV) (400 ng/μL) as described

before (16). The vesicles were collected by centrifugation at 14,000 × *g* for 5 min at 25 °C and the pellets were analyzed by SDS/PAGE. For pull-down experiments, $MinD^{D40A}\Delta10$ and MinE-6xHis were incubated in 1xATPase buffer (25 mM Hepes-NaOH, pH 7.5, 50 mM KCl, and 5 mM $MgCl_2$) in the presence of ADP or ATP (1 mM) for 10 min at 25 °C. The reactions were loaded onto Ni-NTA column (Qiagen) and washed once with 1× ATPase buffer containing 20 mM imidazole. The proteins were eluted with 1× ATPase buffer containing 250 mM imidazole and analyzed by SDS/PAGE.

Measurement of MinD ATPase Activity. MinD (5 μM) and MinE-6xHis (5 μM) or $MinE^{D45A/V49A}$-6xHis (5 μM) were incubated in 1× ATPase buffer (25 mM Hepes-NaOH, pH 7.5, 50 mM KCl, and 5 mM $MgCl_2$) containing MLV (400 ng/μL) in the presence of ATP (1 mM) for 30 min at 25 °C. For quantitative analysis of ATP hydrolysis, a colorimetric assay kit that measures the release of inorganic phosphate (P_i) was used according to the manufacturer's instructions (Innova Biosciences).

Microscopy. Plasmid pSEB104CDE (P_{BAD}::*minC minD minE*) or its derivatives were transformed into JS964 (Δ*min*). A single colony was inoculated into LB containing spectinomycin and 0.2% arabinose and cultured overnight at 37 °C. The next day, each culture was further diluted 1,000-fold and cultured until exponential phase. Samples from each culture were mounted onto an agarose pad containing 1% agarose and 50% LB. A Nikon E600 phase contrast microscope equipped with a CoolSNAP HQ2 CCD camera (Photometrics) was used for photography.

β-Galactosidase Assay. A *cya*-null strain BTH101 Δ*min* was transformed with plasmids pCT25-MinD and pUT18-MinE or derivatives carrying various *minD* and *minE* alleles. Transformants were selected at 37 °C on LB plates containing 0.2% glucose, chloramphenicol (20 μg/mL), and ampicillin (100 μg/mL). The next day, three colonies were picked from each plate and cultured overnight at 30 °C in LB medium containing 0.2% glucose, 20 μg/mL chloramphenicol, and 100 μg/mL ampicillin. The cultures were then diluted 1/100 into fresh LB medium containing 0.5 mM IPTG, 20 μg/mL chloramphenicol, and 100 μg/mL ampicillin and cultured for 3–4 h at 30 °C with growth monitored at OD_{600}. Cells were permeabilized with 0.0016% SDS (wt/vol) and 2.5% chloroform (vol/vol) and vigorously vortexed. Thereafter, 0.4 mL of the permeabilized cells were mixed with 0.6 mL of Z buffer (60 mM Na_2HPO_4, 40 mM NaH_2PO4, pH 7.5, 1 mM $MgSO_4$, and 50 mM β-mercaptoethanol) and 0.25 mL of ONPG (*o*-nitrophenyl β-d-galactopyranoside, 4 mg/mL) (Sigma) was added. The reactions were incubated for an additional 20 min at 25 °C and stopped with 400 mM Na_2CO_3. OD_{420} and OD_{550} values were recorded and converted into Miller activity units as described (14).

HDX-MS. HDX was initiated by making a ∼1:10 dilution of WT or the DM of MinE (to a final protein concentration of 0.5 mg/mL) in 50 mM Hepes, pD-corrected for equivalent pH of 6.8, at 10 °C. At different times after mixing, aliquots of the exchange reactions (3.2 μL) were quenched by the addition of 40 μL of ice-cold 200 mM $(NH4)_3PO_4$ (pH 2.35) containing pepsin A (0.5 mg/mL). Each sample was immediately injected into the HPC loop at −2 °C for a 2-min digestion using a custom-built cooling chamber to reduce back exchange (29).

Initial peptide identification was performed as above, but in the absence of D_2O. The resulting peptic peptides from the digestion were loaded on and on-line reversed phase C18 column (Zorbax C8SB Wide Pore Guard Column, 1 cm × 0.32 mm; Micro-Tech Scientific) and desalted for 4 min at a flow rate of 100 μL/min. Following desalting, peptides were eluted with an acetonitrile gradient (0–90% in 15 min) at a flow rate of 20 μL/min and directed to a linear trap quadrupole-Fourier transform (FT) (Thermo Finnigan) mass spectrometer. Peptides were identified by automatic search analysis of their collision-induced dissociation spectra using Sequest HT algorithm included in Proteome Discoverer (version 1.4) against the sequence of the protein and common contaminants.

Deuterated sample were analyzed in a similar manner, with the omission of the tandem mass analysis, and only ion cyclotron resonance FT scans were used. Hydrogen–deuterium exchange was measured using HDExaminer (Sierra Analytics) H/D exchange kinetics were fit using SigmaPlot version to a two-parameter exponential:

$$D = N_1\left(1 - e^{-k_1 t}\right) + N_2\left(1 - e^{-k_2 t}\right),$$

where D is the deuterium content at time t, N_1 and N_2 are the number of fast and slow exchanging hydrogens, respectively, and k_1 and k_2 are the respective rate constants. All data were acquired with a minimum of two replicates.

ACKNOWLEDGMENTS. This work was funded by NIH Grant GM29764 (to J.L.).

1. Lutkenhaus J (2007) Assembly dynamics of the bacterial MinCDE system and spatial regulation of the Z ring. *Annu Rev Biochem* 76:539–562.
2. de Boer PA, Crossley RE, Hand AR, Rothfield LI (1991) The MinD protein is a membrane ATPase required for the correct placement of the *Escherichia coli* division site. *EMBO J* 10:4371–4380.
3. Huang J, Cao C, Lutkenhaus J (1996) Interaction between FtsZ and inhibitors of cell division. *J Bacteriol* 178:5080–5085.
4. Lackner LL, Raskin DM, de Boer PA (2003) ATP-dependent interactions between *Escherichia coli* Min proteins and the phospholipid membrane in vitro. *J Bacteriol* 185: 735–749.
5. Hu Z, Saez C, Lutkenhaus J (2003) Recruitment of MinC, an inhibitor of Z-ring formation, to the membrane in *Escherichia coli*: Role of MinD and MinE. *J Bacteriol* 185: 196–203.
6. Hu Z, Mukherjee A, Pichoff S, Lutkenhaus J (1999) The MinC component of the division site selection system in *Escherichia coli* interacts with FtsZ to prevent polymerization. *Proc Natl Acad Sci USA* 96:14819–14824.
7. Raskin DM, de Boer PA (1999) MinDE-dependent pole-to-pole oscillation of division inhibitor MinC in *Escherichia coli*. *J Bacteriol* 181:6419–6424.
8. Hu Z, Lutkenhaus J (1999) Topological regulation of cell division in *Escherichia coli* involves rapid pole to pole oscillation of the division inhibitor MinC under the control of MinD and MinE. *Mol Microbiol* 34:82–90.
9. Raskin DM, de Boer PA (1999) Rapid pole-to-pole oscillation of a protein required for directing division to the middle of *Escherichia coli*. *Proc Natl Acad Sci USA* 96:4971–4976.
10. Hale CA, Meinhardt H, de Boer PA (2001) Dynamic localization cycle of the cell division regulator MinE in *Escherichia coli*. *EMBO J* 20:1563–1572.
11. Fu X, Shih YL, Zhang Y, Rothfield LI (2001) The MinE ring required for proper placement of the division site is a mobile structure that changes its cellular location during the *Escherichia coli* division cycle. *Proc Natl Acad Sci USA* 98:980–985.
12. Kruse K, Howard M, Margolin W (2007) An experimentalist's guide to computational modelling of the Min system. *Mol Microbiol* 63:1279–1284.
13. Hu Z, Lutkenhaus J (2001) Topological regulation of cell division in *E. coli*. Spatiotemporal oscillation of MinD requires stimulation of its ATPase by MinE and phospholipid. *Mol Cell* 7:1337–1343.
14. Wu W, Park KT, Holyoak T, Lutkenhaus J (2011) Determination of the structure of the MinD-ATP complex reveals the orientation of MinD on the membrane and the relative location of the binding sites for MinE and MinC. *Mol Microbiol* 79:1515–1528.
15. Hu Z, Gogol EP, Lutkenhaus J (2002) Dynamic assembly of MinD on phospholipid vesicles regulated by ATP and MinE. *Proc Natl Acad Sci USA* 99:6761–6766.
16. Park KT, et al. (2011) The Min oscillator uses MinD-dependent conformational changes in MinE to spatially regulate cytokinesis. *Cell* 146:396–407.
17. Loose M, Kruse K, Schwille P (2011) Protein self-organization: Lessons from the min system. *Annu Rev Biophys* 40:315–336.
18. Ghasriani H, et al. (2010) Appropriation of the MinD protein-interaction motif by the dimeric interface of the bacterial cell division regulator MinE. *Proc Natl Acad Sci USA* 107:18416–18421.
19. King GF, et al. (2000) Structural basis for the topological specificity function of MinE. *Nat Struct Biol* 7:1013–1017.
20. Shih YL, Fu X, King GF, Le T, Rothfield L (2002) Division site placement in *E.coli*: Mutations that prevent formation of the MinE ring lead to loss of the normal midcell arrest of growth of polar MinD membrane domains. *EMBO J* 21:3347–3357.
21. Zhou H, Lutkenhaus J (2005) MinC mutants deficient in MinD- and DicB-mediated cell division inhibition due to loss of interaction with MinD, DicB, or a septal component. *J Bacteriol* 187:2846–2857.
22. Hsieh CW, et al. (2010) Direct MinE-membrane interaction contributes to the proper localization of MinDE in *E. coli*. *Mol Microbiol* 75:499–512.
23. Pascal BD, Chalmers MJ, Busby SA, Griffin PR (2009) HD desktop: An integrated platform for the analysis and visualization of H/D exchange data. *J Am Soc Mass Spectrom* 20:601–610.
24. Zheng M, et al. (2014) Self-assembly of MinE on the membrane underlies formation of the MinE ring to sustain function of the *Escherichia coli* Min system. *J Biol Chem* 289: 21252–21266.
25. Karimova G, Pidoux J, Ullmann A, Ladant D (1998) A bacterial two-hybrid system based on a reconstituted signal transduction pathway. *Proc Natl Acad Sci USA* 95: 5752–5756.
26. Loose M, Fischer-Friedrich E, Herold C, Kruse K, Schwille P (2011) Min protein patterns emerge from rapid rebinding and membrane interaction of MinE. *Nat Struct Mol Biol* 18:577–583.
27. Vecchiarelli AG, et al. (2016) Membrane-bound MinDE complex acts as a toggle switch that drives Min oscillation coupled to cytoplasmic depletion of MinD. *Proc Natl Acad Sci USA* 113:E1479–E1488.
28. Eng NF, Szeto J, Acharya S, Tessier D, Dillon JA (2006) The C-terminus of MinE from *Neisseria gonorrhoeae* acts as a topological specificity factor by modulating MinD activity in bacterial cell division. *Res Microbiol* 157:333–344.
29. Villar MT, Miller DE, Fenton AW, Artigues A (2010) SAIDE: A semi-automated interface for hydrogen/deuterium exchange mass spectrometry. *Proteomica* 6:63–69.